CORONAVIRUS

MBD2 serves as a viable target against pulmonary fibrosis by inhibiting macrophage M2 program

Yi Wang[1]*, Lei Zhang[1]*, Guo-Rao Wu[1], Qing Zhou[1], Huihui Yue[1], Li-Zong Rao[1,2], Ting Yuan[1,2], Biwen Mo[2], Fa-Xi Wang[1], Long-Min Chen[1], Fei Sun[1], Jia Song[1], Fei Xiong[1], Shu Zhang[1], Qilin Yu[1], Ping Yang[1], Yongjian Xu[1], Jianping Zhao[1], Huilan Zhang[1†], Weining Xiong[1,3†], Cong-Yi Wang[1†]

Despite past extensive studies, the mechanisms underlying pulmonary fibrosis (PF) still remain poorly understood. Here, we demonstrated that lungs originating from different types of patients with PF, including coronavirus disease 2019, systemic sclerosis–associated interstitial lung disease, and idiopathic PF, and from mice following bleomycin (BLM)–induced PF are characterized by the altered methyl-CpG–binding domain 2 (MBD2) expression in macrophages. Depletion of Mbd2 in macrophages protected mice against BLM-induced PF. *Mbd2* deficiency significantly attenuated transforming growth factor–β1 (TGF-β1) production and reduced M2 macrophage accumulation in the lung following BLM induction. Mechanistically, Mbd2 selectively bound to the *Ship* promoter in macrophages, by which it repressed Ship expression and enhanced PI3K/Akt signaling to promote the macrophage M2 program. Therefore, intratracheal administration of liposomes loaded with *Mbd2* siRNA protected mice from BLM-induced lung injuries and fibrosis. Together, our data support the possibility that MBD2 could be a viable target against PF in clinical settings.

INTRODUCTION

Pulmonary fibrosis (PF) is a type of chronic, progressive, and irreversible lung interstitial disease, which poses a huge threat to public health (*1*). Some patients develop PF with identifiable triggers such as systemic sclerosis–associated interstitial lung disease (SSc-ILD) (*2*) and 2019 novel coronavirus disease (COVID-19) (*3*), while in some with unknown origins, a term "idiopathic" is applied (IPF) (*2*). Despite significant advances over the past few decades, the molecular mechanisms underlying PF remain poorly understood (*4*, *5*), which rendered its treatment largely unsuccessful. Macrophages are crucially important sentinels integral to host pulmonary defense (*6*, *7*) characterized by their plasticity and diversity (*8*). They are either polarized to the classically activated phenotype (M1) (*9*) or an alternatively activated phenotype (M2) depending on their resided microenvironment (*10*). Previous studies including ours demonstrated that macrophages, particularly M2 macrophages, contribute to the pathogenesis of PF (*6*, *11*). M2 macrophages are a major source of transforming growth factor–β1 (TGF-β1) and platelet-derived growth factor, which, in turn, induce the differentiation of fibroblast into myofibroblast to initiate PF (*12*). Therefore, the number and phenotype of macrophages are thought to be crucial for PF pathological processes (*13*, *14*).

There is compelling evidence that DNA methylation, one of the major epigenetic mechanisms, is involved in the pathogenesis of PF (*15*, *16*). It has been well recognized that the information encoded by DNA methylation is read by a family of methyl-CpG–binding domain (MBD) proteins (i.e., MBD1, MBD2, MBD3, MBD4, and MeCP2) (*17*). Each of these proteins, with the exception of MBD3, mediates transcriptional repression or activation by directly binding to the methylated CpG DNA and recruiting proteins to form a suppressive complex (*18*). Among these proteins, MBD2 has been shown to have the highest binding activity to methylated CpG DNA. Therefore, MBD2 has been recognized to be involved in the pathogenesis of tumorigenesis (*19*), autoimmunity (*20*, *21*), ischemic injury (*22*), obesity (*17*), and neuronal degeneration (*23*).

MBD2 was also found to be highly expressed in macrophages in the lungs derived from patients with COVID-19, SSc-ILD, or IPF and mice following bleomycin (BLM)–induced PF. Moreover, loss of *Mbd2* in macrophages significantly protected mice from BLM-induced PF along with a marked reduction of M2 macrophage accumulation in the lung. Mechanistically, Mbd2 selectively bound to the methylated CpG DNA in the *SH2-containing inositol 5′-phosphatase* (*Ship*) promoter, by which it regulated phosphatidylinositol 3-kinase (PI3K)/Akt signaling to enhance macrophage M2 program. Therefore, intratracheal administration of liposomes carrying *Mbd2* small interfering RNAs (siRNAs) significantly protected mice from BLM-induced PF by targeting macrophage M2 program.

RESULTS

MBD2 is overexpressed in pulmonary fibrotic lungs with different pathoetiologies

We first examined MBD2 expression in fibrotic lungs with different origins. MBD2 was almost undetectable in the lung sections originated from normal controls, but it was highly expressed in the lungs originated from patients with SSc-ILD (Fig. 1A) and IPF (Fig. 1B), while coimmunostaining of CD206 suggested that MBD2 was predominantly colocalized in M2 macrophages, and immunohistochemical staining further confirmed this observation (fig. S1). Next, we checked MBD2 expression in fibrotic lungs derived from severe case of patients with COVID-19 (*24*). As expected, COVID-19 virus could be detected in the lung sections (Fig. 1C), and hematoxylin

[1]The Center for Biomedical Research, NHC Key Laboratory of Respiratory Diseases, Department of Respiratory and Critical Care Medicine, Tongji Hospital, Tongji Medical College, Huazhong University of Sciences and Technology, 1095 Jiefang Ave., Wuhan 430030, China. [2]Department of Respiratory and Critical Care Medicine, The Second Affiliated Hospital of Guilin Medical University, 212 Renmin Road, Guilin 541000, China. [3]Department of Respiratory Medicine, Shanghai Ninth People's Hospital, Shanghai Jiaotong University School of Medicine, 639 Zhizaoju Lu, Shanghai 200011, China.
*These authors contributed equally to this work.
†Corresponding author. Email: wangcy@tjh.tjmu.edu.cn (C.-Y.W.); xiongdoctor@qq.com (W.X.); huilanz_76@163.com (H.Z.)

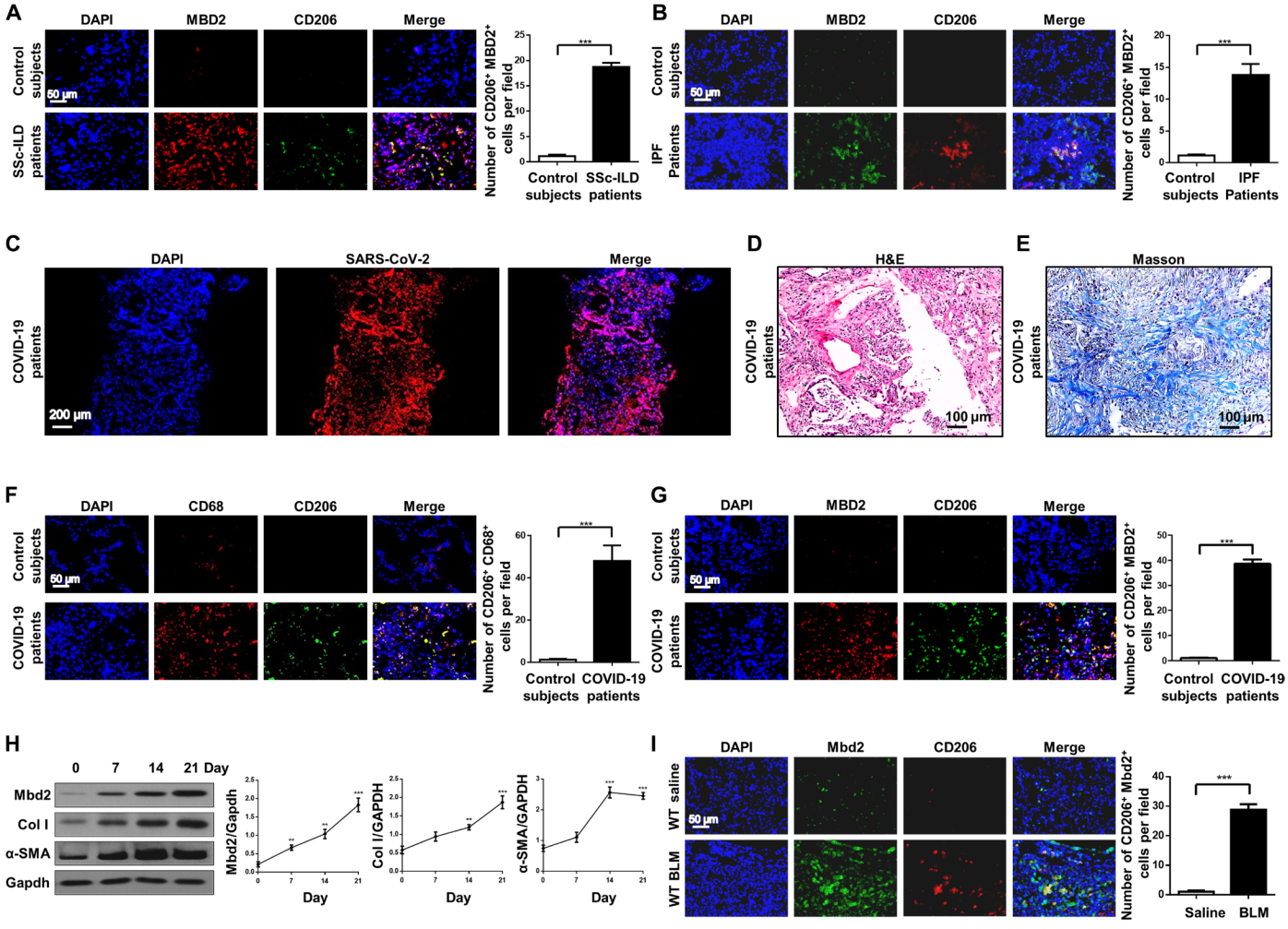

Fig. 1. Analysis of MBD2 expression in patients with PF and mice with BLM induction. (**A** and **B**) Representative results for coimmunostaining of MBD2 and CD206 in the lung sections from patients with SSc-ILD (A) and IPF (B). DAPI, 4′,6-diamidino-2-phenylindole. (**C**) Representative results for immunostaining of severe acute respiratory syndrome coronavirus 2 (SARS-CoV-2) in the lung sections from patients with COVID-19. The images were taken under original magnification of ×100. (**D**) Histological analysis [hematoxylin and eosin (H&E)] of the lung sections from patients with COVID-19. The images were taken under original magnification of ×200. (**E**) Histological analysis (Masson) of the lung sections from patients with COVID-19. The images were taken under original magnification of ×200. (**F**) Representative results for coimmunostaining of CD68 (a macrophage marker) and CD206 (an M2 marker) in the lung sections from patients with COVID-19. (**G**) Representative results for coimmunostaining of MBD2 and CD206 in the lung sections from patients with COVID-19. (**H**) Western blot analysis of Mbd2 and collagen I and α-SMA expression in the lungs of mice following BLM induction. Gapdh, glyceraldehyde-3-phosphate dehydrogenase. (**I**) Results for coimmunostaining of Mbd2 and CD206 in BLM-induced lung sections. The nuclei were stained blue by DAPI, and the images were taken under original magnification of ×400. A total of two patients with COVID-19, three patients with SSc-ILD, eight patients with IPF, and six control subjects were analyzed. Five mice were analyzed in each group. Col I, collagen I. The data are represented as the means ± SD. $^{**}P < 0.01$ and $^{***}P < 0.001$.

and eosin (H&E) and Masson staining indicated the existence of inflammatory infiltration (Fig. 1D) and PF (Fig. 1E). In particular, lungs from patients with COVID-19 were also featured by the significant M2 macrophage infiltration (Fig. 1F), along with MBD2 overexpression in M2 macrophages (Fig. 1G). Collectively, these findings suggest that altered MBD2 expression in M2 macrophages could be a common feature in PF with different pathological origins.

To address the above assumption, we further examined Mbd2 expression in the lungs of mice following BLM-induced fibrosis. It was noted that BLM time-dependently induced Mbd2 overexpression in the lung. Specifically, an eightfold Mbd2 overexpression was noted in the fibrotic lungs following day 21 of BLM induction, along with increased expression of collagen I and α–smooth muscle actin (α-SMA), markers for PF (Fig. 1H). Moreover, the progression of PF was highly correlated with the severity of M2 macrophage accumulation and the levels of Mbd2 overexpression in the lungs (Fig. 1I). Together, our data support that PFs with different origins are characterized by the induction of MBD2 overexpression in M2 macrophages.

Mbd2 deficiency protects mice against BLM-induced lung injury and fibrosis

To dissect the role of MBD2 in the pathogenesis of PF, we generated a macrophage-specific *Mbd2* knockout (KO) mouse model, which selectively deleted *Mbd2* in macrophages (the *LyzM-Cre*$^{+}$-*Mbd2*$^{flox/flox}$ mice, hereinafter defined as *Mbd2-CKO* mice), and their littermates

(the *LyzM-Cre*$^{-}$-*Mbd2*$^{flox/flox}$ mice, hereinafter defined as *Mbd2-C* mice) were served as controls (Fig. 2A). *Mbd2* depletion was confirmed by genotyping of the tail blood DNA for the presence of the *flox* allele (indicated by arrows in fig. S2A), along with the detection of *Cre* allele (fig. S2B). Coimmunostaining of lung sections validated *Mbd2* deficiency in F4/80^{+} macrophages in *Mbd2-CKO* mice evidenced by the absence of Mbd2 colocalization with macrophages observed in *Mbd2-C* mice (Fig. 2B).

The *Mbd2-CKO* and *Mbd2-C* mice were subjected to assess the severity of PF 21 days following BLM challenge. Significantly attenuated lung injury and fibrosis were noted in *Mbd2-CKO* mice as illustrated by the H&E, Sirius red, and Masson's trichrome staining (Fig. 2C, left). Phenotypically, the severity of PF was much lower in *Mbd2-CKO* mice as demonstrated by the lower fibrotic scores (Fig. 2C, right). In line with these observations, higher severity of fibrosis in *Mbd2-C* mice was characterized by the higher levels of hydroxyproline than that in *Mbd2-CKO* mice (Fig. 2D). Consistently, Western blot analysis confirmed a significant reduction in the expression of fibronectin, collagen I, and α-SMA in the lungs derived from *Mbd2-CKO* mice (Fig. 2E), and similar data were also obtained by reverse transcription polymerase chain reaction (RT-PCR) analysis (Fig. 2F). Consistent with published data (*25*), the LyzM-Cre expression alone did not affect macrophage M2 program and BLM-induced PF (fig. S3). Together, our data support that specific loss of *Mbd2* in macrophages protects mice against BLM-induced lung injury and fibrosis.

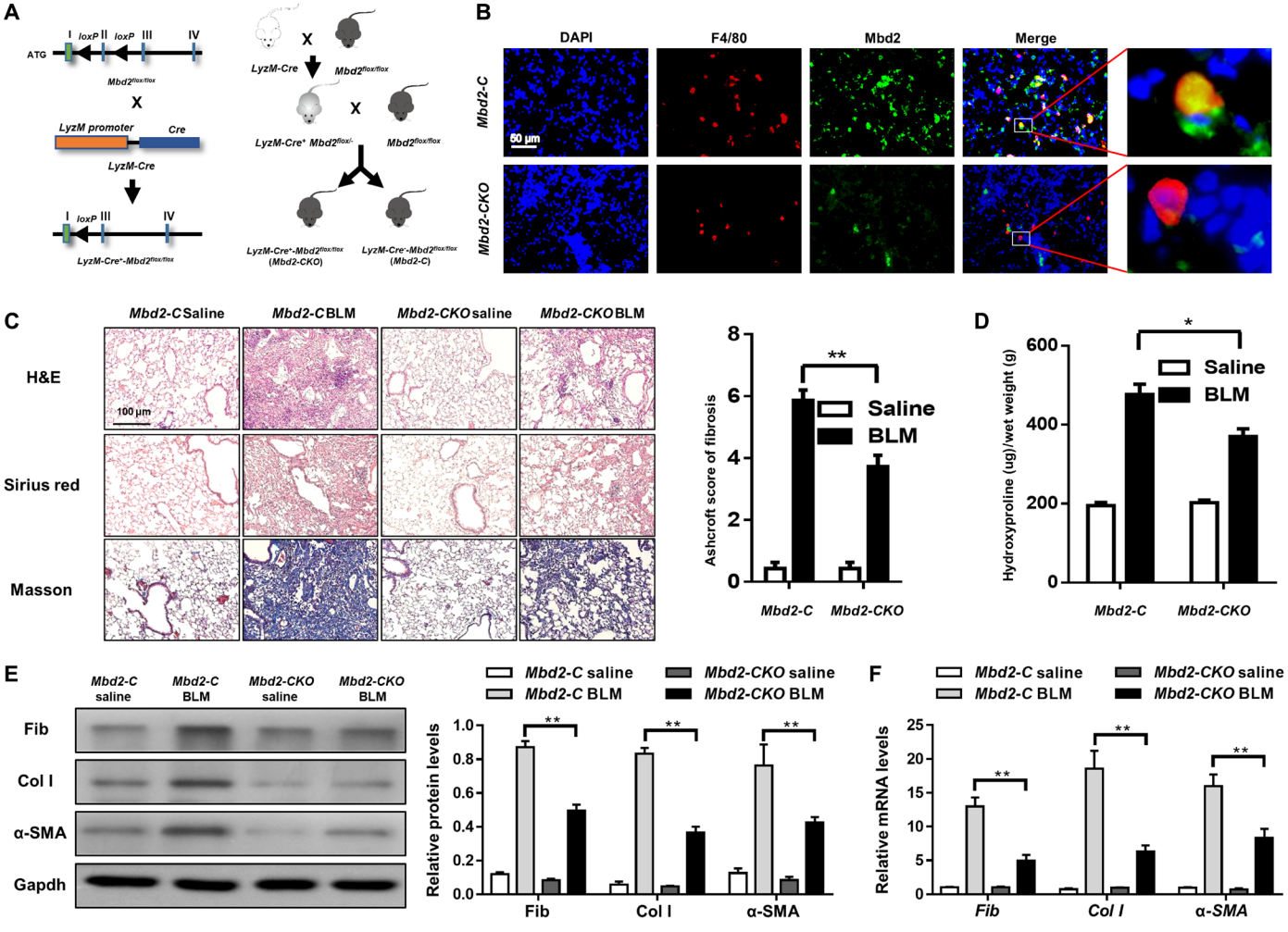

Fig. 2. Comparison of the severity of lung fibrosis between *Mbd2-C* and *Mbd2-CKO* mice after BLM induction. (**A**) *Mbd2*$^{flox/flox}$ mice were generated by inserting two loxP sequences in the same direction into the introns flanked with the exon 2 of MBD2 based on the CRISPR-Cas9 system, which could produce a nonfunctional MBD2 protein by generating a stop codon in exon 3 after Cre-mediated gene deletion. *Mbd2*$^{flox/flox}$ was then crossed with the *LyzM-Cre* transgenic mice to get the macrophage-specific *Mbd2*-knockout mice, which were named as *LyzM-Cre*$^{+}$-*Mbd2*$^{flox/flox}$. (**B**) Representative results for coimmunostaining of F4/80 and Mbd2 in the lung sections from *Mbd2*-C and *Mbd2*-CKO mice. Nuclei were stained blue by DAPI, and the images were taken at an original magnification of ×400. (**C**) Histological analysis of the severity of lung fibrosis in mice after BLM induction. Left: representative images for H&E (top), Sirius red (middle), and Masson staining (bottom). Right: a bar graph figure showing the quantitative mean score of the severity of fibrosis. Images were captured at ×200 magnification. (**D**) Quantification of hydroxyproline contents in *Mbd2-C* and *Mbd2-CKO* mice after BLM challenge. (**E**) Western blot analysis of fibronectin, collagen I, and α-SMA. (**F**) RT-PCR analysis of *fibronectin*, *collagen I*, and α-*SMA*. Seven mice were included in each study group. BLM, bleomycin; Col I, collagen I; Fib, fibronectin. The data are represented as the means ± SD. *$P < 0.05$ and **$P < 0.01$.

Mbd2 deficiency suppresses TGF-β signaling

Given the critical role of TGF-β1 played in the initiation and progression of PF, we examined TGF-β1 expression in the lung. Impressively, *Mbd2-CKO* mice displayed much lower levels of TGF-β1 expression both at protein (Fig. 3A) and mRNA (Fig. 3B) levels than that of lungs from *Mbd2-C* mice following BLM induction. These results rendered us to further check the TGF-β1 downstream signaling molecules. Significantly higher levels of phosphorylated Smad2 (p-Smad2) and p-Smad3 were detected in the BLM-induced lungs originated from *Mbd2-C* mice than that from *Mbd2-CKO* mice, while no perceptible difference in terms of total Smad2/3 was observed (Fig. 3C). Moreover, *Tgfbr1* and *Tgfbr2*, the two major TGF-β1 receptors, did not show a substantial difference in mRNA levels between lungs from *Mbd2-C* and *Mbd2-CKO* mice following BLM challenge (Fig. 3, D and E), indicating that the reduced Smad signaling is likely caused by the decreased TGF-β1 expression in *Mbd2-CKO* mice. Immunostaining revealed that TGF-β1 was predominantly localized in the infiltrated macrophages after BLM induction as determined by F4/80 costaining (Fig. 3F). Collectively, our data suggest that *Mbd2* deficiency attenuates the capacity of macrophages for secretion of TGF-β1, thereby repressing Smad2/3 signaling following BLM induction.

Mbd2 deficiency attenuates the M2 program in macrophages

The above results prompted us to embark on the impact of *Mbd2* deficiency on macrophage M2 program. To confirm the immunostaining results (Fig. 1I), lung F4/80$^+$ cells were subjected to flow cytometry analysis as described following BLM induction. *Mbd2-CKO* mice manifested a significantly lower percentage of lung M2 macrophages (F4/80$^+$CD206$^+$) than that of *Mbd2-C* mice, but *Mbd2* deficiency did not seem to affect the induction of M1 macrophages as we failed to detect a perceptible difference in terms of the number of F4/80$^+$CD11c$^+$ macrophages (Fig. 4A). Consistently, Western blot analysis of BLM-induced lung homogenates revealed a 2.6-fold reduction in the expression of M2 marker Arg 1 in *Mbd2-CKO* mice as compared to the *Mbd2-C* mice (Fig. 4B), and RT-PCR analysis of two additional M2 markers, *found in inflammatory zone 1* (*Fizz1*; Fig. 4C) and *chitinase 3–like 3* (*YM1*; Fig. 4D), demonstrated similar results.

To further dissect the mechanism underlying Mbd2 regulation of macrophage M2 program, bone marrow–derived macrophages (BMDMs) were generated from *Mbd2-C* and *Mbd2-CKO* mice and then subjected to interleukin-4 (IL-4) stimulation. IL-4 induced significantly higher levels of mean fluorescence intensity for CD206 in *Mbd2-C* BMDMs than that in *Mbd2-CKO* BMDMs (Fig. 4E), and a substantial increase in Mbd2 protein expression was noted upon IL-4 stimulation in *Mbd2-C* BMDMs, while Arg 1 was decreased in *Mbd2-CKO* BMDMs as compared to *Mbd2-C* BMDMs following IL-4 induction (Fig. 4F). RT-PCR analysis of two other M2 markers, *Fizz1* (Fig. 4G) and *YM1* (Fig. 4H), revealed similar results. Next, *Mbd2-CKO* BMDMs were transduced with mock or Mbd2 lentiviruses followed by IL-4 stimulation. As expected, compared to mock-transduced BMDMs, Mbd2-transduced cells were featured by the significantly increased expression of Arg 1 during the course of IL-4 stimulation (fig. S4). Notably, consistent with previous data in the lung, *Mbd2* deficiency did not affect the induction of M1 macrophages (Fig. 4I) and *IL-6* expression (Fig. 4J) following lipopolysaccharide (LPS) and interferon-γ (IFN-γ) stimulation, suggesting that Mbd2 might selectively modulate the M2 program in macrophages.

The above results support the assumption that *Mbd2* deficiency protects mice against BLM-induced lung injury and fibrosis depending on the repression of macrophage M2 program. To address this question, we first compared disease severity after depletion of macrophages. Clodronate liposomes were intratracheally administered to deplete macrophages in the lungs of *Mbd2-CKO* and *Mbd2-C* mice, and mice administered with liposomes were served as controls. Of note, similar to published data (*11*), macrophages were almost undetectable in the bronchoalveolar lavage fluid (BALF) of clodronate liposome–treated mice, along with a significant reduction in the number of total cells (fig. S5). Therefore, 1 day after depletion of

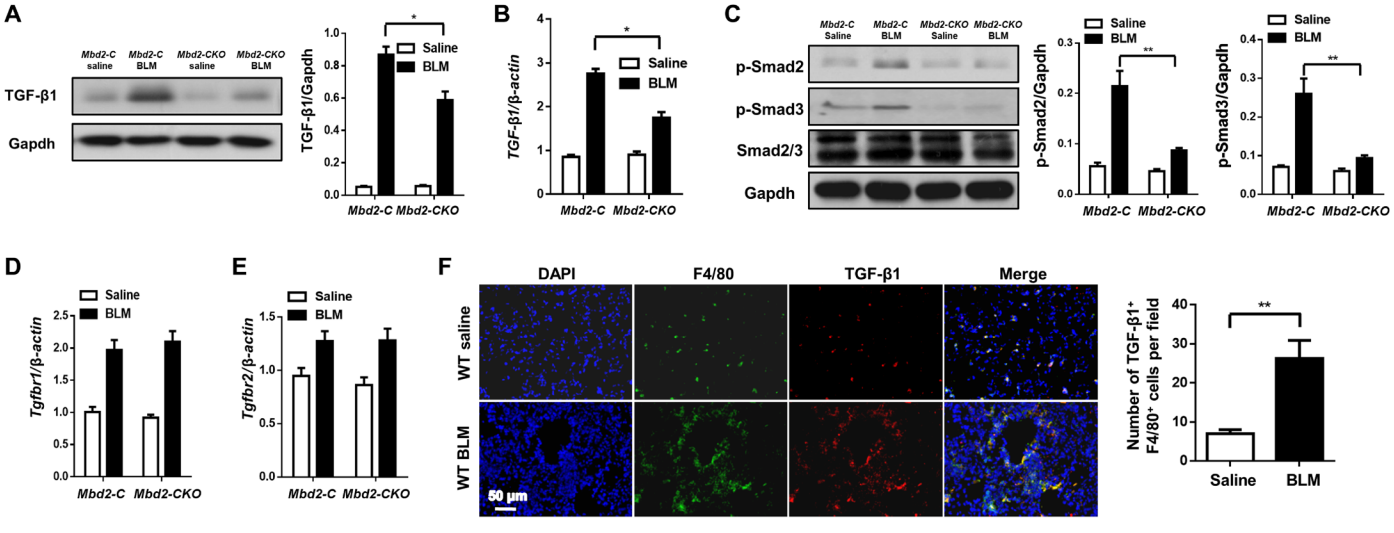

Fig. 3. *Mbd2* deficiency repressed TGF-β/Smad signaling after BLM induction. (**A**) Western blot analysis of TGF-β1 expression in the lung homogenates. (**B**) Real-time PCR results for *TGF-β1* expression in the lungs after BLM induction. (**C**) Western blot analysis of p-Smad2, p-Smad3, and Smad2/3 expression. Real-time PCR results for *Tgfr1* (**D**) and *Tgfr2* (**E**) expression in the lungs after BLM induction. (**F**) Coimmunostaining of TGF-β1 and F4/80 in the lung sections of WT mice. The images were taken under original magnification of ×400. Each bar represents the means ± SD of seven mice studied. *$P < 0.05$ and **$P < 0.01$.

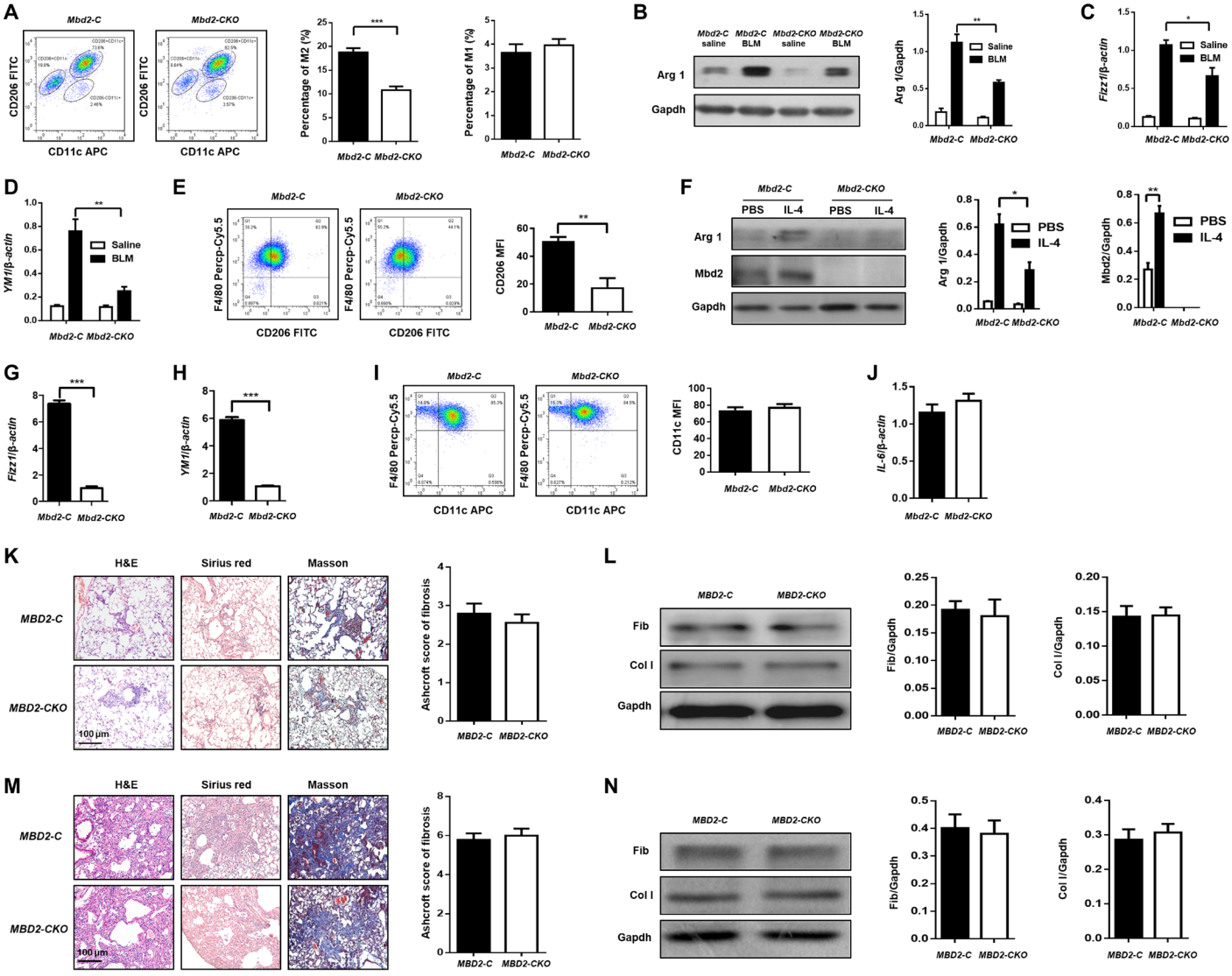

Fig. 4. Mbd2 was overexpressed by the infiltrated M2 macrophages in the lung following BLM induction. (**A**) Flow cytometry analysis of macrophages derived from lung tissues of *Mbd2-C* and *Mbd2-CKO* mice after BLM induction. FITC, fluorescein isothiocyanate. (**B**) Results for Arg 1 expression in the lung homogenates. Real-time PCR results for analysis of *Fizz1* (**C**) and *YM1* (**D**) expression in the lung. (**E**) Flow cytometry analysis of CD206 expression in BMDMs following IL-4 stimulation. (**F**) Results for Arg 1 and Mbd2 expression in the BMDMs after IL-4 induction. PBS, phosphate-buffered saline. Real-time PCR for analysis of *Fizz1* (**G**) and *YM1* (**H**) expression in the BMDMs after IL-4 induction. (**I**) Flow cytometry analysis of CD11c expression in BMDMs. (**J**) Real-time PCR analysis of *IL-6* expression. (**K**) The severity of PF in *Mbd2-C* and *Mbd2-CKO* mice after depletion of macrophages. Left: representative results for H&E, Sirius red, and Masson staining. Right: a bar graph figure showing the semiquantitative Ashcroft scores for the severity of fibrosis. (**L**) Levels of fibronectin and collagen I in the lungs of macrophage-depleted *Mbd2-C* and *Mbd2-CKO* mice after BLM induction. (**M**) Results for adoptive transfer of WT macrophages into *Mbd2-C* and *Mbd2-CKO* mice following BLM induction. Left: representative results for H&E, Sirius red, and Masson staining. Right: the semiquantitative Ashcroft scores relevant to the severity of fibrosis. (**N**) Western blotting for analysis of collagen I and fibronectin expression. All images were captured at ×200 magnification, and seven mice were included in each study group. Arg 1, arginase 1; BMDMs, bone marrow–derived macrophages; Fizz1, found in inflammatory zone 1; YM1, chitinase 3–like 3; Col I, collagen I; Fib, fibronectin; MFI, mean fluorescence intensity. The data are represented as the means ± SD. $^{*}P < 0.05$, $^{**}P < 0.01$, and $^{***}P < 0.001$.

macrophages, the mice were induced for PF with BLM, respectively. As expected, *Mbd2-CKO* mice displayed comparable disease severity with that of *Mbd2-C* mice (Fig. 4, K and L). Higher disease severity was noted in *Mbd2-CKO* mice treated with liposomes as compared to that of *Mbd2-CKO* mice treated with clodronate liposomes (fig. S6). Next, BMDMs from *Mbd2-C* mice were treated with IL-4 to induce M2 macrophages, and 1×10^6 M2 macrophages were adoptively transferred through intratracheal injection into clodronate liposome–treated *Mbd2-C* and *Mbd2-CKO* mice on day 7 of BLM induction. Same as above, adoptive transfer of wild-type (WT) M2 macrophages significantly impaired the protective effect conferred by *Mbd2* deficiency in *Mbd2-CKO* mice (Fig. 4, M and N). Together, these results suggest that *Mbd2* deficiency protects mice from BLM-induced lung injury and fibrosis dependent on its suppressive effect on macrophage M2 polarization.

Depletion of Mbd2 represses PI3K/Akt signaling to attenuate M2 program

It is believed that PI3K/AKT and signal transducers and activators of transcription 6 (STAT6)/peroxisome proliferator–activated receptor γ (PPAR-γ) signaling are critical for the optimal and sustained macrophage M2 program upon IL-4 or IL-13 stimulation (*26*, *27*). We then compared temporal expression changes in terms of PI3K/AKT and STAT6/PPAR-γ signaling between *Mbd2-CKO* and *Mbd2-C* BMDMs following IL-4 stimulation. No significant difference was observed for total P85 or Akt between *Mbd2-C* and *Mbd2-CKO* macrophages. The phosphorylated P85 (p-P85) and p-Akt were relatively low in both types of macrophages before IL-4 stimulation, while a time-dependent increase was observed upon IL-4 stimulation. However, much higher levels of p-P85 and p-Akt (i.e., p-Ser^{473} and p-Thr^{308}) were detected in *Mbd2-C* BMDMs as compared to *Mbd2-CKO* BMDMs, and IL-4 also time-dependently upregulated Mbd2 expression (Fig. 5A). Similarly, higher levels of p-P85 and p-AKT were detected in patients with IPF as well (fig. S7A). Unlike its effect on PI3K/Akt signaling, no significant difference in terms of p-STAT6 and PPAR-γ was detected between *Mbd2-C* and *Mbd2-CKO* BMDMs following IL-4 stimulation (Fig. 5B).

It has been reported that SHIP, inositolpolyphosphate 4-phosphatase type II (Inpp4B), and phosphatase and tensin homolog (Pten) were critical for PI3K/Akt signaling by hydrolyzing or inhibiting the activity of PI-3,4,5-P3 (*28*, *29*). *Mbd2-C* BMDM manifested a onefold lower *Ship* expression than that of *Mbd2-CKO* BMDMs (Fig. 5C). However, *Mbd2* deficiency in macrophages did not seem to affect the expression of *Inpp4b* and *Pten* (Fig. 5, D and E).

As MBD2 acts as a reader to interpret DNA methylome–encoded information, we thus next conducted studies to check global DNA

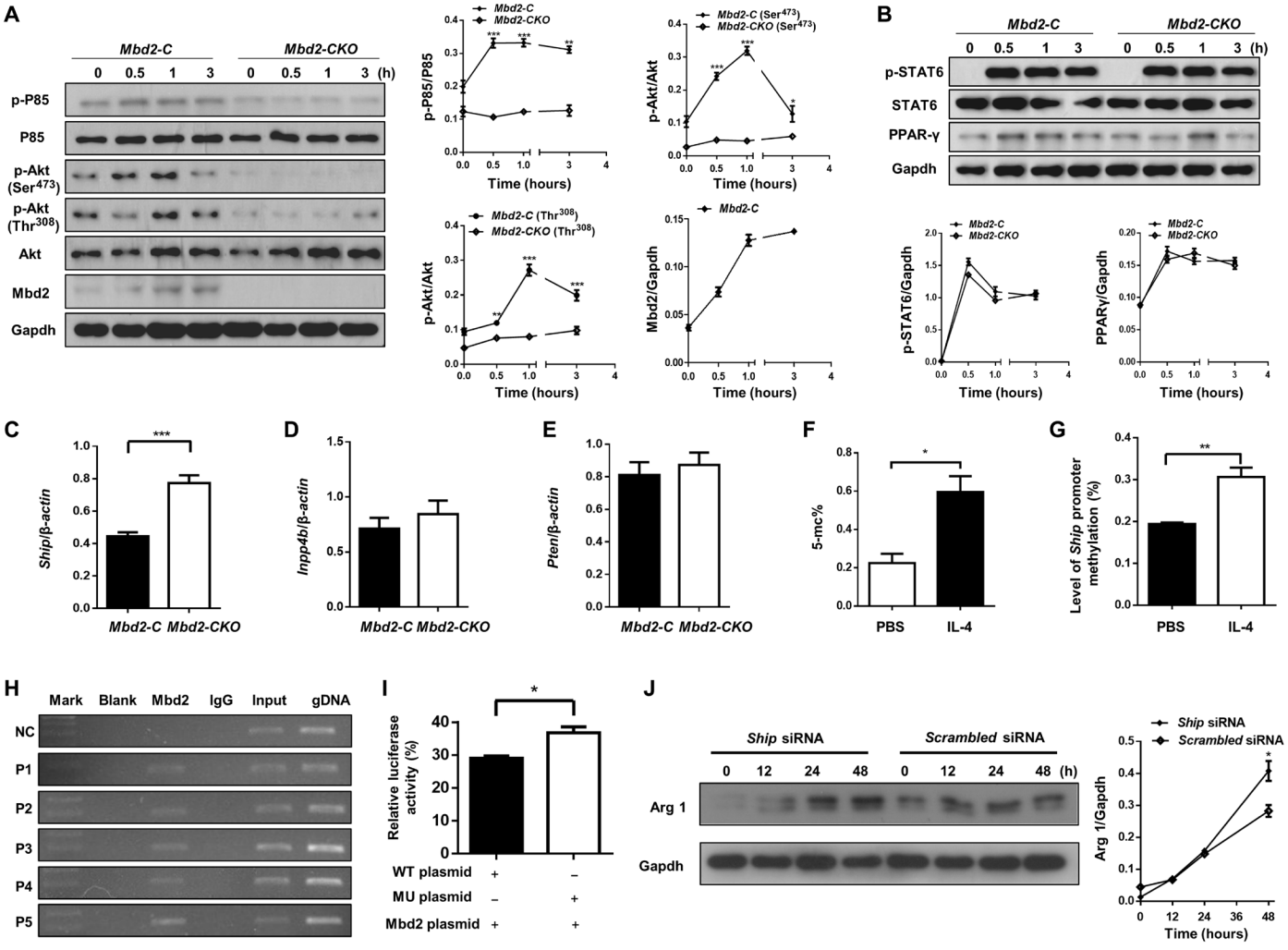

Fig. 5. Loss of *Mbd2* attenuated IL-4–induced PI3K/Akt signaling in macrophages. (**A**) Analysis of IL-4–induced PI3K/Akt signaling in macrophages. (**B**) Results for time course Western blot analysis of STAT6, p-STAT6, and PPAR-γ expression in BMDM following IL-4 stimulation. Real-time PCR for analysis of *Ship* (**C**), *Inpp4b* (**D**), and *Pten* (**E**) expression in IL4-induced BMDMs. (**F**) Global DNA methylation rate in BMDMs after IL-4 treatment. (**G**) Results for the bisulfite DNA sequencing analysis of the *Ship* promoter. (**H**) ChIP results for the analysis of Mbd2 binding activity to the *Ship* promoter. The distal region of *Ship* promoter [−1770 to −1540 base pairs (bp)] was served as a negative control. gDNA, guide DNA; MU, mutant. (**I**) Relative luciferase activity in BMDMs. (**J**) Results for a time course Western blot analysis of Arg 1 expression in IL-4–induced *Mbd2-CKO* BMDMs transfected with *Scrambled* or *Ship* siRNA. Ship, SH2-containing inositol 5′-phosphatase; Arg 1, arginase 1; NC, negative control. The data are represented as the means ± SEM. **P* < 0.05, ***P* < 0.01, and ****P* < 0.001.

methylation levels and *Ship* promoter methylation state in macrophages. Unlike reduced global DNA methylation levels in fibrotic lung genomic DNA, IL-4 induced a global genomic DNA hypermethylation in BMDMs (Fig. 5F). Particularly, IL-4 induced the *Ship* promoter to undergo a DNA hypermethylation (Fig. 5G), and similar results were noted in patients with IPF as well (fig. S7B). The next key question is whether Mbd2 selectively binds to the above hypermethylated CpG DNA within the *Ship* promoter. Chromatin immunoprecipitation (ChIP) was then used to address this question. Mbd2 selectively bound to the methylated CpG DNA in five regions (from −1336 to +167 base pairs, the transcriptional start site as +1; fig. S8) within the *Ship* promoter, while ChIP-PCR yielded negative result in the distal region absent of CpG DNA (Fig. 5H). Furthermore, DNA methylation–dependent luciferase reporter assays confirmed that the transcriptional activity of Ship was higher in the BMDMs with mutant plasmid (no methylated DNA) than those with the WT plasmid (with methylated DNA; Fig. 5I). Suppression of *Ship* by siRNA in *Mbd2-CKO* BMDMs restored their capability for M2 polarization following IL-4 stimulation (Fig. 5J). Collectively, our data support that MBD2 binds to the *Ship* promoter to repress its expression, by which it enhances PI3K/Akt signaling to promote macrophage M2 program.

Intratracheal administration of *Mbd2* siRNA liposomes protects mice against BLM-induced PF

Last, we sought to translate the above discoveries into a therapeutic approach against PF. To this end, we generated lipid-based liposomes loaded with an *Mbd2* siRNA (fig. S9A). The prepared liposomes displayed >90% entrapment efficiency for loading siRNA with a zeta potential of 3.2 mV (fig. S9B). A representative image was then taken by transmission electron microscope (TEM; fig. S9C), and those liposomes manifested a normal distribution of hydrodynamic diameter (fig. S9D) with sustained stability within 24 hours (fig. S9E). Next, Cell Counting Kit-8 assay was used to check the effect of liposome-loaded siRNA on cell viability of BMDMs, and we failed to detect any toxicity of liposome-loaded siRNA in cell viability with different concentrations (fig. S9F). To assess the safety of liposome in vivo, we conducted H&E staining and terminal deoxynucleotidyl transferase–mediated deoxyuridine triphosphate nick end labeling assay of lung sections following intratracheal liposome administration. As expected, administration of liposomes did not induce inflammation in the lung and epithelial apoptosis (fig. S9, G and H). To demonstrate the biodistribution of liposomes, In Vivo Imaging System (IVIS) was used to track the fluorescent signal of lipophilic carbocyanine $DiOC_{18}(7)$ (DiR)–labeled liposomes. Encouragingly, those intratracheal administered liposomes sustainably accumulated in the lung for at least 7 days (Fig. 6A). To further confirm this observation, organs such as heart, liver, spleen, lung, and kidney were collected from four mice after day 7 of intratracheal injection of liposomes and then subjected to analysis of near-infrared fluorescent (NIRF) signals. As expected, NIRF signals were only detected in the lungs but absent in other organs (Fig. 6B).

Next, the distribution of liposomes in the lung tissues was further explored in a BLM-induced mouse model. Unexpectedly, liposomes were predominantly located in the fibrotic area of lung tissues and could be mainly overlapped with $F4/80^+$ macrophages but not prosurfactant protein C $(pro\text{-}SPC)^+$ epithelial cells, indicating a high efficiency for their uptake by macrophages (Fig. 6C and fig. S10). To further address the effect of siRNA-loaded liposomes on protein expression in lung tissues, we examined Mbd2 expression changes in the lungs following liposome-based pulmonary delivery. Of note, a significant decrease in Mbd2 expression was noted after intratracheal delivery of *Mbd2* siRNA–loaded liposomes, and the nadir was detected at day 3 after the treatment. Nevertheless, this expression was returned to normal levels at day 7 (Fig. 6D).

Last, the therapeutic effect of siRNA-loaded liposomes was assessed in mice following BLM induction. WT mice were administrated with *Scrambled* or *Mbd2* siRNA–loaded liposomes at day 14 and day 18 (1 mg/kg; intratracheal), respectively (Fig. 6E). Administration of *Mbd2* siRNA–loaded liposomes significantly alleviated BLM-induced lung injury and fibrosis as illustrated by the histopathological analysis (Fig. 6F, left) and fibrotic scores (Fig. 6F, right). Consistently, mice administered with *Mbd2* siRNA–loaded liposomes displayed much lower levels of hydroxyproline in the lung (Fig. 6G), coupled with a significant reduction in the expression of fibrotic markers (fibronectin, collagen I, and α-SMA) and macrophage M2 marker, Arg 1 (Fig. 6H). Together, our data support that intratracheal administration of *Mbd2* siRNA–loaded liposomes could be a viable therapy against PF in clinical settings.

DISCUSSION

In the present report, we conducted studies in patients and animals to address the impact of MBD2, a reader for interpreting DNA methylation–encoded information, on the pathogenesis of PF. Lungs originating from different types of patients with PF and from mice following BLM-induced PF were characterized by altered MBD2 expression. Specifically, MBD2 was overexpressed in infiltrated M2 macrophages within the lung during course of fibrotic processes. Therefore, depletion of *Mbd2* in macrophages protected mice from BLM-induced lung injury and PF. In general, macrophages are characterized by the DNA hypermethylation in the fibrotic lungs. As a result, Mbd2 binds to the methylated CpG DNA within the *Ship* promoter to inhibit *Ship* expression, by which Mbd2 enhances PI3K/Akt signaling to promote macrophage M2 program. M2 macrophages, in turn, secrete a large amount of TGF-β1, which then activates fibroblasts to initiate and promote fibrotic processes (Fig. 6I). Mice with macrophage-specific *Mbd2* deficiency are characterized by the reduced TGF-β1 production, along with attenuated Smad2/3 signaling following BLM challenge. Together, our results support that strategies aimed at silencing MBD2 in macrophages could be a viable therapy against PF in clinical settings.

In general, PF is featured by idiopathic in nature with possible genetic predisposition. However, it can also be recognized as a complication of connective tissue disease or with certain environmental, occupational, or drug exposures. For example, PF is a common consequence in certain patients following COVID-19 infection (*30*, *31*). Unfortunately, no effective pharmacological therapy against PF, thus far, is available other than lung transplantation. In this report, we demonstrated evidence that macrophages originated from fibrotic lungs of patients with COVID-19 and SSc-ILD or IPF are featured by the overexpression of MBD2, a methylated DNA binding protein. Those observations are consistent with previous studies (*32*), in which patients with PF manifest a DNA methylation turnover characterized by the changes of methylation patterns for the target genes and/or methylation levels for a particular gene. For example, the levels of DNA methylation enzymes such as DNMT3a and DNMT3b, and MBD proteins such as MeCP2, are highly elevated

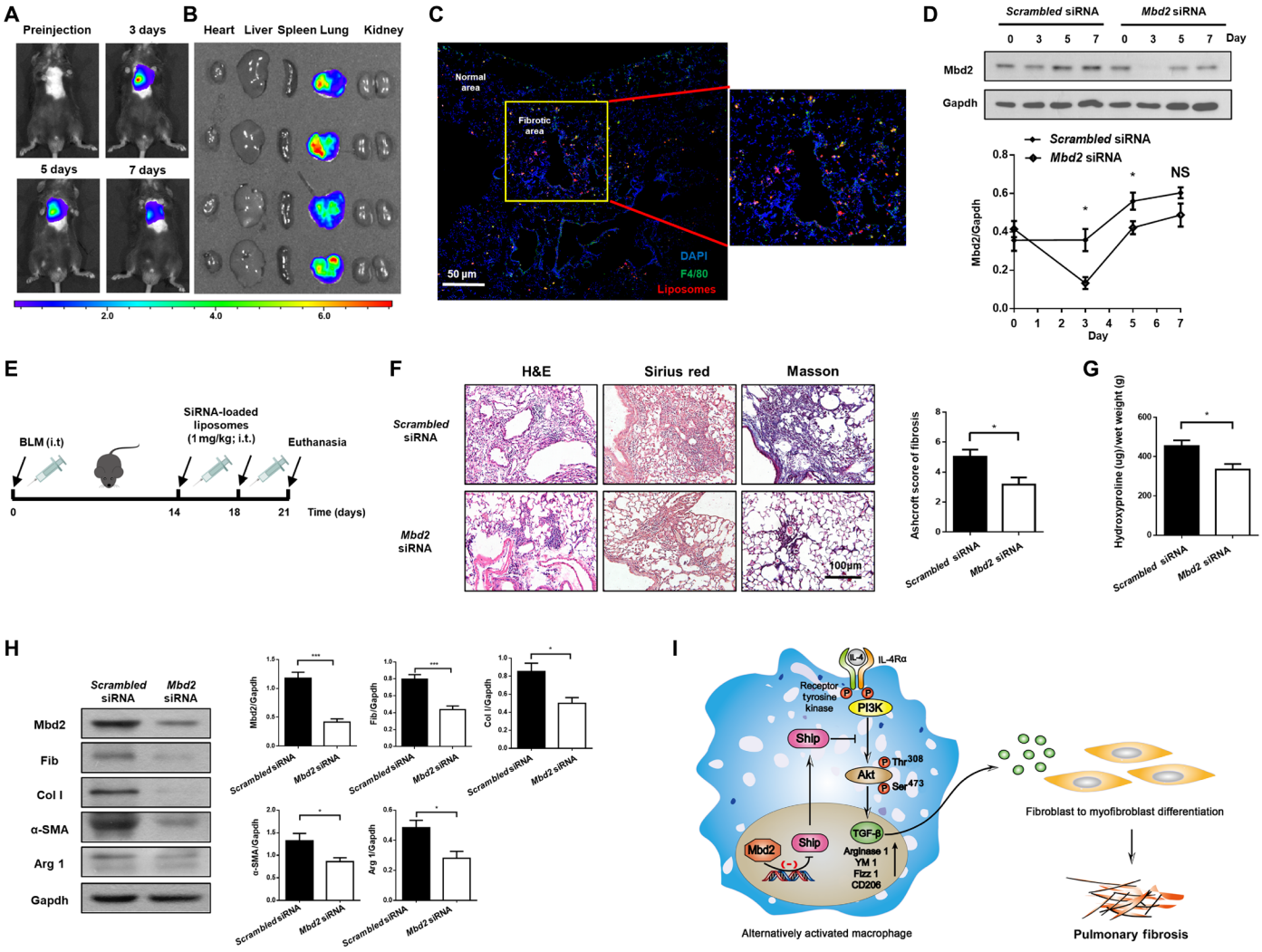

Fig. 6. Intratracheal administration of Mbd2 siRNA–loaded liposomes protected mice from BLM-induced lung injury and fibrosis. (**A**) Representative IVIS images of the mouse administrated with DiR-labeled liposomes. (**B**) Ex vivo fluorescence images of major organs from mice. (**C**) Confocal immunofluorescence image for the biodistribution of liposomes in lungs from BLM-induced mice. Images were captured at ×200 magnification. (**D**) Temporal Mbd2 expression changes in the lungs from liposome administered mice, and four mice were included in each study group. (**E**) Schematic for experimental design and time line of BLM-treated WT mice administered with either *Scrambled* or *Mbd2* siRNA–loaded liposomes. (**F**) Intratracheal administration of *Mbd2* siRNA–loaded liposomes provided protection for mice against BLM-induced lung injury and fibrosis. Left: representative results for H&E, Sirius red, and Masson staining. Right: the semiquantitative Ashcroft scores relevant to the severity of fibrosis. Images were captured at ×200 magnification. (**G**) Quantification of hydroxyproline contents in mice after BLM challenge. Six mice were included in each study group. (**H**) Western blot analysis of Mbd2, fibronectin, collagen I, α-SMA, and Arg 1 expression in the lungs. (**I**) Mbd2 selectively bound to the *Ship* promoter in macrophages, by which it repressed *Ship* expression and enhanced PI3K/Akt signaling to promote macrophage M2 program. Upon activation, M2 macrophages secreted high levels of TGF-β1 into the milieu of lung fibroblasts, which then induced the progression of PF. i.t., intratracheal injection; Col I, collagen I; Fib, fibronectin; Arg 1, arginase 1. The data are represented as the means ± SD. **P* < 0.05 and ****P* < 0.001.

in the lungs of patients with IPF, which were associated with up-regulation of fibrotic genes (*15*, *33*). Collectively, these data support that DNA methylation is implicated in PF pathogenesis, and MBD2 serves as a reader of methylated DNA contributing to PF development.

The most exciting discovery in this report is that Mbd2 was noted to regulate macrophage M2 program, which maybe a common factor for the initiation of fibrotic processes. Previous studies suggested that DNA methylation may modulate the activation of M2 macrophages during the course of obesity (*34*). We now provided convincing evidence that loss of MBD2 promotes macrophage M2 polarization. Specifically, we demonstrated that mice with specific deficiency of *Mbd2* in macrophages were significantly protected from BLM-induced lung injury and fibrosis, which were abolished once macrophages were depleted or *Mbd2*-*C* M2 macrophages were adoptively transferred into the lung. Moreover, MBD2 only selectively regulates macrophage M2 program, without a perceptible impact on M1 macrophages. In addition, we also observed that loss of *Mbd2* in macrophages did not affect the total number of macrophages in the lung (fig. S11). It was noted that IL-4 stimulates the *Ship* promoter in macrophages to undergo a DNA hypermethylation, along with MBD2 overexpression, and MBD2, in turn, binds to the methylated CpG DNA within the *Ship* promoter to suppress its expression. DNA methylation–dependent promoter reporter assays confirmed that MBD2 significantly suppressed *Ship* transcription. The attenuated

Ship expression would then release its suppressive effect on the PI3K/Akt signaling (*35*), which is essential to activate and sustain macrophage M2 program (*36*). Of note, our macrophage depletion and adoptive transfer studies further confirmed that the reduced M2 macrophages contribute to the protective effect on PF conferred by *Mbd2* deficiency. As a result, mice deficient in *Mbd2* are manifested by the significant reduction of M2 macrophages in the lung following BLM induction.

Given the fact that no effective therapy is currently available for PF, numerous clinical trials have been carried out to characterize viable drugs (*37*, *38*). For this purpose, properties for a particular drug, such as half-life in the blood, concentrations in the lungs, and possible side effects on other organs and tissues, are necessary for consideration. Therefore, drug administration directly through tracheal inhalation rather than systemic delivery could be a better approach for patients with PF. Liposomes are established drug carriers for inhalation owing to their safety and ability to provide controlled drug release in the lung. These carriers can entrap a wide range of therapeutic molecules for delivery in large volumes to the peripheral airways using medical nebulizers (*39*, *40*). A unique delivery system with nanostructured lipid carriers through inhalation of prostaglandin E2 coupled with MMP3 siRNAs, CCL12 (chemokine), and hypoxia-inducible factor 1A has been used to limit lung injuries in patients with PF and to prevent disease progression by suppressing the synthesis of pro-fibrotic proteins (*41*, *42*). Similarly, our studies in this report demonstrated that liposomes carrying the *Mbd2* siRNA could be efficiently uptaken by the macrophages in fibrotic lesions of the lung following intratracheal injection. The liposome-based repression of Mbd2 expression lasted for a week or so. As a result, intratracheal delivery of liposomes carrying the *Mbd2* siRNA protected mice from BLM-induced lung injury and fibrosis.

Immunostaining of lung sections from BLM-induced fibrotic mice also noted MBD2 overexpression in certain cells other than F4/80$^+$ macrophages (Fig. 3F), while analysis of IPF single-cell sequencing data suggested that those cells were fibroblasts and epithelial cells (fig. S12). Given that this report selectively focused on macrophages, the impact of altered MBD2 expression in fibroblasts and epithelial cells on PF would be tackled in our future studies.

In summary, we have demonstrated that lungs originating from patients with PF and from mice following BLM-induced PF are characterized by the altered MBD2 expression. Therefore, mice with macrophages deficient in *Mbd2* are protected from BLM-induced lung injury and fibrosis. MBD2 selectively binds to the methylated CpG DNA within the *Ship* promoter in macrophages, by which it represses *Ship* expression and enhances PI3K/Akt signaling to promote the macrophage M2 program. Since MBD2 itself does not affect DNA methylation and appears not to be essential for biological processes under physiological conditions (*17*, *20*, *22*), MBD2 could be, therefore, a viable target against PF. Intratracheal administration of liposomes carrying the *Mbd2* siRNA substantially protected mice from BLM-induced lung injuries and fibrosis. Together, our data support the possibility that intratracheal administration of liposome-based *MBD2* siRNA could be a viable therapy against PF in clinical settings.

MATERIALS AND METHODS

Human samples

Lung tissues from patients with non–small cell lung cancer (n = 6), COVID-19 (n = 2), SSc-ILD (n = 3), and IPF (n = 8) were collected in the Tongji Hospital with informed consent. COVID-19 was diagnosed by nucleic acid test (*43*), SSc-ILD was classified according to the American College of Rheumatology (ACR)/European League Against Rheumatism (EULAR) criteria (*44*), and the IPF diagnosis was made according to the American Thoracic Society (ATS)/European Respiratory Society (ERS) consensus diagnostic criteria (*45*). The studies were approved by the Human Assurance Committee of the Tongji Hospital. Clinical data and pulmonary function tests were provided in table S1.

BLM induction of PF

Mbd2$^{flox/flox}$ mice were generated using the CRISPR-Cas9 system by the Bioray Laboratories Inc. (Shanghai, China). Two *loxP* sequences were inserted in the introns flanked with the *exon 2* of MBD2 as described in Fig. 2A. The *LyzM-Cre* transgenic mice were purchased from the Jackson laboratory (Bar Harbor, ME, USA) and bred into C57BL/6 background by backcrossing with WT C57BL/6 mice for more than 12 generations. *LyzM-Cre*$^+$-*Mbd2*$^{flox/flox}$ (*Mbd2-CKO*) mice were generated by crossing the *LyzM-Cre* mice with *Mbd2*$^{flox/flox}$ mice for specific deletion of Mbd2 in macrophages, and their littermates *LyzM-Cre*$^-$-*Mbd2*$^{flox/flox}$ (*Mbd2-C*) were used as controls. WT C57BL/6 mice were derived from the Jackson laboratory. *Mbd2-C* and *Mbd2-CKO* mice (8 to 10 weeks old) were anesthetized with 1% pentobarbital sodium (60 mg/kg) and then intratracheally administered BLM (0.5 mg/kg; Nippon Kayaku, Tokyo, Japan) in 40 μl of normal saline (*11*). Mice administered with same volume of normal saline served as controls. siRNA-loaded liposomes were injected into the anesthetized animals via intratracheal on the days 14 and 18 after BLM injection. The mice were euthanized on day 21 following BLM challenge to analyze PF. All mice were housed in an specific pathogen-free (SPF) facility at the Tongji Medical College with a 12-hour light/12-hour dark cycle. All experimental procedures were approved by the Animal Care and Use Committee at the Tongji Hospital.

Fluorescent images were acquired on an IVIS Lumina XR system (Caliper Life Sciences, Hopkinton, USA) equipped with a 150-W quartz halogen lamp and a 1-mW power scanning laser. The following parameters were used: exposure time of 0.5 s, binning of 1, and f/stop of 2. Filter sets were fixed with the following parameters: excitation wavelength at 640 nm and emission wavelength at 670 nm. Acquired images were measured and analyzed by the Living Imaging software.

Reagents and antibodies

Murine recombinant IL-4 was obtained from PeproTech (London, UK). Antibodies against collagen type I was purchased from EMD Millipore (Schwalbach, Germany). Antibodies against fibronectin, α-SMA, arginase-1, CD68, MBD2, and pro-SPC were purchased from Abcam (Cambridge, MA, USA), and antibodies against p-Smad2, p-Smad3, STAT6, P85, p-P85, and p-Akt (Thr^{308}) were obtained from Cell Signaling Technology (Danvers, MA, USA). Antibodies against MBD2, glyceraldehyde-3-phosphate dehydrogenase, p-Akt (Ser^{473}), and p-STAT6 were obtained from Santa Cruz Biotechnology (Santa Cruz, CA, USA). Anti-mouse F4/80-PerCP/Cy5.5 and CD206–fluorescein isothiocyanate (FITC) were from BioLegend (San Diego, CA, USA), and CD11c–allophycocyanin (APC) were purchased from BD Biosciences (San Jose, CA, USA). Lipidoid (C12-200) was purchased from Xinjiahecheng Medical Chemistry Corporation (Wuhan, Hubei, China). mPEG2000-DEG was purchased from NOF Corporation (Tokyo, Japan). All other reagents were purchased from Sigma-Aldrich (St Louis, MO, USA), unless otherwise stated.

Histological and immunohistochemical analysis

The left lung was inflated and placed in fresh 4% neutral-buffered paraformaldehyde for 24 hours at room temperature, embedded in paraffin, and subjected to the histological analysis as previously reported (*17*). Each successive field was individually assessed for the severity of interstitial fibrosis in a blinded fashion by two pathologists using the Ashcroft scoring system (*46*). For immunostaining, the frozen sections (7 μm) were probed with antibodies against CD206, CD68, Mbd2, and F4/80, followed by staining with Alexa Fluor 594–labeled anti-mouse/rabbit or Alexa Fluor 488–conjugated anti-rabbit/mouse antibodies (Invitrogen, Carlsbad, CA, USA), respectively. COVID-19 viral immunostaining was conducted as previously reported (*47*).

Culture and treatment of BMDMs

BMDMs were obtained from male mice as reported (*48*, *49*). Red blood cells in bone marrow samples were lysed and then resuspended in 50 ml of culture medium consisting of RPMI 1640, 10% fetal bovine serum (FBS), penicillin/streptomycin, and macrophage colony-stimulating factor (30 ng/ml). The cells were next plated in 35 mm by 15 mm tissue culture dishes at 37°C, and the medium was changed every 2 days. After 7 days, the differentiated macrophages were cocultured with IL-4 (10 ng/ml) at the indicated time points.

Macrophage depletion and adoptive transfer studies

Clodronate liposomes (40 μl) were intratracheally administered for two successive days before BLM induction, and the severity of PF was assessed 21 days after BLM induction (*11*). For adoptive transfer studies, WT naive BMDMs were first stimulated with IL-4 (10 ng/ml) for 12 hours to induce M2 macrophages and then transferred into the lungs of clodronate liposome–treated *Mbd2-C* and *Mbd2-CKO* mice at a density of 1×10^6 cells per mouse (50 μl) at day 7 of BLM induction through intratracheal injection. The mice were sacrificed 2 weeks after the adoptive transfer for fibrotic analysis.

Western blot analysis

Lung tissues and cultured cells were homogenized in radioimmunoprecipitation assay lysis buffer (Beyotime, Shanghai, China), and equal amounts of lysates were separated on 10% polyacrylamide gels (Sigma-Aldrich) and transferred onto polyvinylidene difluoride membranes. The membranes were next probed with indicated primary antibodies for analysis of protein levels as described (*50*).

Quantitative RT-PCR analysis

Quantitative RT-PCR was performed using the SYBR Premix Ex Taq (TaKaRa, Tokyo, Japan), and the relative expression of each target gene was normalized by β-actin as previously described (*51*, *52*). The following primers were used for each target gene: *Fibronectin* (5′-ATG CAA CGA TCA GGA CAC AA-3′ and 5′-TGT GCC TCT CAC ACT TCC AC-3′), *Collagen I* (5′-CCT GGT AAA GAT GGT GCC-3′ and 5′-CAC CAG GTT CAC CTT TCG CAC C-3′), α-*SMA* (5′-CGT ACA ACT GGT ATT GTG CTG GAC-3′ and 5′-TGA TGT CAC GGA CAA TCT CAC GCT-3′), *YM1* (5′-GGG CAT ACC TTT ATC CTG AG-3′ and 5′-CCA CTG AAG TCA TCC ATG TC-3′), *Fizz1* (5′-TCC CAG TGA ATA CTG ATG AGA-3′ and 5′-CCA CTC TGG ATC TCC CAA GA-3′), *Ship* (5′-GAG ACA CTG TTT CAG CGT CTA C-3′ and 5′-CGT CTT CAA AAA GTC GGA ATC CA-3′), *Inpp4B* (5′-TCC AGA AGA TTC CGA ACG AGC-3′ and 5′-GTT TCC GAT CAC TGA CAG GAG-3′), *Pten* (5′-TGG ATT CGA CTT AGA CTT GAC CT-3′ and 5′-GCG GTG TCA TAA TGT CTC TCA G-3′), *Mbd2* (5′-GGA GGA AGT GAT CCG AAA ATC AG-3′ and 5′-AGC ATT TCC CAG GTA TCT TGC-3′), and β-*actin* (5′-TGA CGT TGA CAT CCG TAA AGA CC-3′ and 5′-CTC AGG AGG AGC AAT GAT CTT GA-3′). Relative expression levels for each target gene were calculated using the $2^{-\Delta\Delta Ct}$ method.

ChIP assay and *Ship* promoter reporter assay

ChIP assays were conducted using the ChIP Assay Kit (Beyotime, Shanghai, China) as reported (*8*). Briefly, 1×10^6 WT BMDMs were cross-linked with formaldehyde, and chromatin fragmentation was carried out according to the protocol provided. The above-prepared diluted soluble chromatin solution was then incubated with an Mbd2 antibody overnight at 4°C with rotation. Normal rabbit immunoglobulin G was used to determine nonspecific bindings. The above mixtures were next incubated with protein A + G agarose beads, and the protein-DNA complexes were eluted out after washes. The eluted DNA was subjected to ChIP-PCR with indicated primers. The primers used for *Ship* in the ChIP assay were as follows: F1, 5′-TCA GAA TGT AGA CGT GAG CTC TTG T-3′; R1, 5′-GCT GTG TTG ATG TCA TCC ATG G-3′; F2, 5′-TCC CAT GTC CTC CAC ACA CCA G-3′; R2, 5′-CAC TCC TTC ATC TGA ACC TTG TCA C-3′; F3, 5′-AAC AAT CAC CAC TTC TGC CGT AAG C-3′; R3, 5′-CCT CTG TGG CTA GAC ATG GCT AT-3′; F4, 5′-GGA AGG TAG ATG ATG CCC CC-3′; R4, 5′-CAG CAA AGT AGT TCA GGG CC-3′; F5, 5′-GAG TGT CCG TCC TGG GAG TGG-3′; and R5, 5′-AGT TGG GAG GAG ACG GGT ACT CAC A-3′. The distal region of the *Ship* promoter absent of CpG DNA was used as a negative control. The primers were F (5′-CAT GAG ATC CAA CTG TAA GGC-3′) and R (5′-CAT ACT GCT GTT CAT CAC CAA-3′). The Dual-Luciferase Reporter System (Promega, Madison, WI) was used for the *Ship* promoter luciferase reporter assays, in which the Mbd2 binding site within the *Ship* promoter was disrupted using the established techniques (*17*).

Global DNA methylation assay and bisulfite DNA sequencing

Global DNA methylation was determined using the MethylFlash Methylated DNA Quantification Kit (Epigentek, NY, USA) as instructed. Bisulfite DNA sequencing was conducted as previously described (*20*).

siRNA transfection

Mbd2-CKO BMDMs cultured in RIPM1640 supplemented with 10% FBS were transfected with a *Ship* siRNA or *Scrambled* siRNA (Ribobio, Guangzhou, China) using the Lipofectamine 3000 reagent (Invitrogen, Carlsbad, CA, USA) as previously described (*53*). The transfected cells were next stimulated with murine IL-4 (10 ng/ml) at indicated time points.

Flow cytometry analysis

Mononuclear cells were isolated from lung tissues using the established techniques (*54*), while BMDMs were stimulated with LPS (100 ng/ml) + IFN-γ (100 U/ml) or IL-4 (10 ng/ml) for 12 hours. The cells were then stained with anti-mouse F4/80-PerCP/Cy5.5 (1:100), CD11c-APC (1:100), and CD206-FITC (1:100) antibodies. After washes, the cells were analyzed using a FACSCanto II (BD

Biosciences, San Jose, CA, USA). All data were analyzed using the FACS Express V3 software (De Novo Software) according to the manufacturer's instructions.

Preparation and characterization of siRNA-loaded liposomes

siRNA-loaded liposomes were prepared as reported (*55*). Briefly, lipidoid, cholesterol, distearoyl phosphatidylcholine (DSPC), and 1,2-dimyristoyl-rac-glycero-3-methoxypolyethylene glycol-2000 (mPEG-DMG) were dissolved in ethanol at a molar ratio of 50:38.5:10:1.5. siRNA was dissolved in citrated buffer (10 mM, pH 3). The lipid components and the dissolved siRNA were then mixed rapidly by vortex. The next step was to exclude unentrapped siRNA by ultrafiltration centrifugation. Last, the siRNA liposomes were diluted in phosphate-buffered saline. Hydrodynamic diameter, polydispersity, zeta potential, and stability of the liposomes were measured by dynamic light scattering (Malvern Zetasizer Nano-ZS, UK). A Ribogreen assay was used to calculate the entrapment efficiency of siRNA. After staining with 2% phosphotungstic acid, the liposomes were characterized by TEM (JEM-1230, Jeol, Japan).

Statistical analysis

Comparisons between groups were undertaken using the Graph Pad Prism (version 5.0) software (GraphPad Software Inc., San Diego, CA, USA). Two experimental groups were compared using a Student's *t* test for paired data or a Student's *t* test with Welch's correction for unpaired data. For comparisons of more than two groups, a one-way analysis of variance (ANOVA) with Bonferroni's correction was used. The data are presented as the means ± SD unless otherwise specified. In all cases, $P < 0.05$ was considered with statistical significance.

SUPPLEMENTARY MATERIALS

Supplementary material for this article is available at http://advances.sciencemag.org/cgi/content/full/sciadv.abb6075/DC1

View/request a protocol for this paper from *Bio-protocol*.

REFERENCES AND NOTES

1. M. J. Schafer, T. A. White, K. Iijima, A. J. Haak, G. Ligresti, E. J. Atkinson, A. L. Oberg, J. Birch, H. Salmonowicz, Y. Zhu, D. L. Mazula, R. W. Brooks, H. Fuhrmann-Stroissnigg, T. Pirtskhalava, Y. S. Prakash, T. Tchkonia, P. D. Robbins, M. C. Aubry, J. F. Passos, J. L. Kirkland, D. J. Tschumperlin, H. Kita, N. K. Le Brasseur, Cellular senescence mediates fibrotic pulmonary disease. *Nat. Commun.* **8**, 14532 (2017).
2. A. McLean-Tooke, I. Moore, F. Lake, Idiopathic and immune-related pulmonary fibrosis: Diagnostic and therapeutic challenges. *Clin. Transl. Immunol.* **8**, e1086 (2019).
3. Y.-H. Xu, J.-H. Dong, W.-M. An, X.-Y. Lv, X.-P. Yin, J.-Z. Zhang, L. Dong, X. Ma, H.-J. Zhang, B.-L. Gao, Clinical and computed tomographic imaging features of novel coronavirus pneumonia caused by SARS-CoV-2. *J. Infect.* **80**, 394–400 (2020).
4. G. Raghu, J. Behr, K. K. Brown, J. J. Egan, S. M. Kawut, K. R. Flaherty, F. J. Martinez, S. D. Nathan, A. U. Wells, H. R. Collard, U. Costabel, L. Richeldi, J. de Andrade, N. Khalil, L. D. Morrison, D. J. Lederer, L. Shao, X. Li, P. S. Pedersen, A. B. Montgomery, J. W. Chien, T. G. O'Riordan; ARTEMIS-IPF Investigators, Treatment of idiopathic pulmonary fibrosis with ambrisentan: A parallel, randomized trial. *Ann. Intern. Med.* **158**, 641–649 (2013).
5. L. Shulgina, A. P. Cahn, E. R. Chilvers, H. Parfrey, A. B. Clark, E. C. F. Wilson, O. P. Twentyman, A. G. Davison, J. J. Curtin, M. B. Crawford, A. M. Wilson, Treating idiopathic pulmonary fibrosis with the addition of co-trimoxazole: A randomised controlled trial. *Thorax* **68**, 155–162 (2013).
6. J. L. Larson-Casey, J. S. Deshane, A. J. Ryan, V. J. Thannickal, A. B. Carter, Macrophage Akt1 kinase-mediated mitophagy modulates apoptosis resistance and pulmonary fibrosis. *Immunity* **44**, 582–596 (2016).
7. J. Mesureur, J. R. Feliciano, N. Wagner, M. C. Gomes, L. Zhang, M. Blanco-Gonzalez, M. van der Vaart, D. O'Callaghan, A. H. Meijer, A. C. Vergunst, Macrophages, but not neutrophils, are critical for proliferation of *Burkholderia cenocepacia* and ensuing host-damaging inflammation. *PLOS Pathog.* **13**, e1006437 (2017).
8. Y. Wang, J. Zhu, L. Zhang, Z. Zhang, L. He, Y. Mou, Y. Deng, Y. Cao, P. Yang, Y. Su, J. Zhao, S. Zhang, Q. Yu, J. Hu, Z. Chen, Q. Ning, X. Xiang, Y. Xu, C.-Y. Wang, W. Xiong, Role of C/EBP homologous protein and endoplasmic reticulum stress in asthma exacerbation by regulating the IL-4/signal transducer and activator of transcription 6/transcription factor EC/IL-4 receptor α positive feedback loop in M2 macrophages. *J. Allergy Clin. Immunol.* **140**, 1550–1561.e8 (2017).
9. T. Kimura, S. Nada, N. Takegahara, T. Okuno, S. Nojima, S. Kang, D. Ito, K. Morimoto, T. Hosokawa, Y. Hayama, Y. Mitsui, N. Sakurai, H. Sarashina-Kida, M. Nishide, Y. Maeda, H. Takamatsu, D. Okuzaki, M. Yamada, M. Okada, A. Kumanogoh, Polarization of M2 macrophages requires Lamtor1 that integrates cytokine and amino-acid signals. *Nat. Commun.* **7**, 13130 (2016).
10. A. J. Byrne, T. M. Maher, C. M. Lloyd, Pulmonary Macrophages: A new therapeutic pathway in fibrosing lung disease? *Trends Mol. Med.* **22**, 303–316 (2016).
11. Y. Yao, Y. Wang, Z. Zhang, L. He, J. Zhu, M. Zhang, X. He, Z. Cheng, Q. Ao, Y. Cao, P. Yang, Y. Su, J. Zhao, S. Zhang, Q. Yu, Q. Ning, X. Xiang, W. Xiong, C.-Y. Wang, Y. Xu, Chop deficiency protects mice against bleomycin-induced pulmonary fibrosis by attenuating M2 macrophage production. *Mol. Ther.* **24**, 915–925 (2016).
12. S. Su, Q. Zhao, C. He, D. Huang, J. Liu, F. Chen, J. Chen, J.-Y. Liao, X. Cui, Y. Zeng, H. Yao, F. Su, Q. Liu, S. Jiang, E. Song, miR-142-5p and miR-130a-3p are regulated by IL-4 and IL-13 and control profibrogenic macrophage program. *Nat. Commun.* **6**, 8523 (2015).
13. A. R. Froese, C. Shimbori, P.-S. Bellaye, M. Inman, S. Obex, S. Fatima, G. Jenkins, J. Gauldie, K. Ask, M. Kolb, Stretch-induced activation of transforming growth factor-β_1 in pulmonary fibrosis. *Am. J. Resp. Crit. Care Med.* **194**, 84–96 (2016).
14. D. V. Pechkovsky, A. Prasse, F. Kollert, K. M. Y. Engel, J. Dentler, W. Luttmann, K. Friedrich, J. Müller-Quernheim, G. Zissel, Alternatively activated alveolar macrophages in pulmonary fibrosis-–mediator production and intracellular signal transduction. *Clin. Immunol.* **137**, 89–101 (2010).
15. Y. Y. Sanders, N. Ambalavanan, B. Halloran, X. Zhang, H. Liu, D. K. Crossman, M. Bray, K. Zhang, V. J. Thannickal, J. S. Hagood, Altered DNA methylation profile in idiopathic pulmonary fibrosis. *Am. J. Resp. Crit. Care Med.* **186**, 525–535 (2012).
16. I. V. Yang, B. S. Pedersen, E. Rabinovich, C. E. Hennessy, E. J. Davidson, E. Murphy, B. J. Guardela, J. R. Tedrow, Y. Zhang, M. K. Singh, M. Correll, M. I. Schwarz, M. Geraci, F. C. Sciurba, J. Quackenbush, A. Spira, N. Kaminski, D. A. Schwartz, Relationship of DNA methylation and gene expression in idiopathic pulmonary fibrosis. *Am. J. Resp. Crit. Care Med.* **190**, 1263–1272 (2014).
17. J. Cheng, J. Song, X. He, M. Zhang, S. Hu, S. Zhang, Q. Yu, P. Yang, F. Xiong, D. W. Wang, J. Zhou, Q. Ning, Z. Chen, D. L. Eizirik, Z. Zhou, C. Zhao, C.-Y. Wang, Loss of *Mbd2* protects mice against high-fat diet-induced obesity and insulin resistance by regulating the homeostasis of energy storage and expenditure. *Diabetes* **65**, 3384–3395 (2016).
18. Q. Du, P.-L. Luu, C. Stirzaker, S. J. Clark, Methyl-CpG-binding domain proteins: Readers of the epigenome. *Epigenomics.* **7**, 1051–1073 (2015).
19. M. Zhou, K. Zhou, L. Cheng, X. Chen, J. Wang, X.-M. Wang, Y. Zhang, Q. Yu, S. Zhang, D. Wang, L. Huang, M. Huang, D. Ma, T. Cheng, C.-Y. Wang, W. Yuan, J. Zhou, MBD2 ablation impairs lymphopoiesis and impedes progression and maintenance of T-ALL. *Cancer Res.* **78**, 1632–1642 (2018).
20. J. Zhong, Q. Yu, P. Yang, X. Rao, L. He, J. Fang, Y. Tu, Z. Zhang, Q. Lai, S. Zhang, M. Kuczma, P. Kraj, J.-F. Xu, F. Gong, J. Zhou, L. Wen, D. L. Eizirik, J. Du, W. Wang, C.-Y. Wang, MBD2 regulates T_H17 differentiation and experimental autoimmune encephalomyelitis by controlling the homeostasis of T-bet/Hlx axis. *J. Autoimmun.* **53**, 95–104 (2014).
21. P. C. Cook, H. Owen, A. M. Deaton, J. G. Borger, S. L. Brown, T. Clouaire, G.-R. Jones, L. H. Jones, R. J. Lundie, A. K. Marley, V. L. Morrison, A. T. Phythian-Adams, E. Wachter, L. M. Webb, T. E. Sutherland, G. D. Thomas, J. R. Grainger, J. Selfridge, A. N. J. Mc Kenzie, J. E. Allen, S. C. Fagerholm, R. M. Maizels, A. C. Ivens, A. Bird, A. S. MacDonald, A dominant role for the methyl-CpG-binding protein Mbd2 in controlling Th2 induction by dendritic cells. *Nat. Commun.* **6**, 6920 (2015).
22. X. Rao, J. Zhong, S. Zhang, Y. Zhang, Q. Yu, P. Yang, M.-H. Wang, D. J. Fulton, H. Shi, Z. Dong, D. Wang, C.-Y. Wang, Loss of methyl-CpG-binding domain protein 2 enhances endothelial angiogenesis and protects mice against hind-limb ischemic injury. *Circulation* **123**, 2964–2974 (2011).
23. M. Santos, T. Summavielle, A. Teixeira-Castro, A. Silva-Fernandes, S. Duarte-Silva, F. Marques, L. Martins, M. Dierssen, P. Oliveira, N. Sousa, P. Maciel, Monoamine deficits in the brain of methyl-CpG binding protein 2 null mice suggest the involvement of the cerebral cortex in early stages of Rett syndrome. *Neuroscience* **170**, 453–467 (2010).
24. N. Chen, M. Zhou, X. Dong, J. Qu, F. Gong, Y. Han, Y. Qiu, J. Wang, Y. Liu, Y. Wei, J. Xia, T. Yu, X. Zhang, L. Zhang, Epidemiological and clinical characteristics of 99 cases of 2019 novel coronavirus pneumonia in Wuhan, China: A descriptive study. *Lancet* **395**, 507–513 (2020).
25. F. Wang, F. Sun, J. Luo, T. Yue, L. Chen, H. Zhou, J. Zhang, C. Yang, X. Luo, Q. Zhou, H. Zhu, J. Li, P. Yang, F. Xiong, Q. Yu, H. Zhang, W. Zhang, A. Xu, Z. Zhou, Q. Lu, D. L. Eizirik, S. Zhang, C.-Y. Wang, Loss of ubiquitin-conjugating enzyme E2 (Ubc9) in macrophages exacerbates multiple low-dose streptozotocin-induced diabetes by attenuating M2 macrophage polarization. *Cell Death Dis.* **10**, 892 (2019).

26. A. J. Covarrubias, H. I. Aksoylar, T. Horng, Control of macrophage metabolism and activation by mTOR and Akt signaling. *Semin. Immunol.* **27**, 286–296 (2015).
27. S. J. Bensinger, P. Tontonoz, Integration of metabolism and inflammation by lipid-activated nuclear receptors. *Nature* **454**, 470–477 (2008).
28. I. U. Agoulnik, M. C. Hodgson, W. A. Bowden, M. M. Ittmann, INPP4B: The new kid on the PI3K block. *Oncotarget* **2**, 321–328 (2011).
29. L. M. Sly, V. Ho, F. Antignano, J. Ruschmann, M. Hamilton, V. Lam, M. J. Rauh, G. Krystal, The role of SHIP in macrophages. *Front. Biosci.* **12**, 2836–2848 (2007).
30. J. Wang, B. J. Wang, J. C. Yang, M. Y. Wang, C. Chen, G. X. Luo, W. F. He, Advances in the research of mechanism of pulmonary fibrosis induced by Corona Virus Disease 2019 and the corresponding therapeutic measures. *Zhonghua Shao Shang Za Zhi* **36**, 691–697 (2020).
31. Z. Ye, Y. Zhang, Y. Wang, Z. Huang, B. Song, Chest CT manifestations of new coronavirus disease 2019 (COVID-19): A pictorial review. *Eur. Radiol.* **30**, 4381–4389 (2020).
32. B. A. Helling, A. N. Gerber, V. Kadiyala, S. K. Sasse, B. S. Pedersen, L. Sparks, Y. Nakano, T. Okamoto, C. M. Evans, I. V. Yang, D. A. Schwartz, Regulation of *MUC5B* expression in idiopathic pulmonary fibrosis. *Am. J. Respir. Cell Mol. Biol.* **57**, 91–99 (2017).
33. B. Hu, M. Gharaee-Kermani, Z. Wu, S. H. Phan, Essential role of MeCP2 in the regulation of myofibroblast differentiation during pulmonary fibrosis. *Am. J. Pathol.* **178**, 1500–1508 (2011).
34. X. Yang, X. Wang, D. Liu, L. Yu, B. Xue, H. Shi, Epigenetic regulation of macrophage polarization by DNA methyltransferase 3b. *Mol. Endocrinol.* **28**, 565–574 (2014).
35. M. J. Rauh, V. Ho, C. Pereira, A. Sham, L. M. Sly, V. Lam, L. Huxham, A. I. Minchinton, A. Mui, G. Krystal, SHIP represses the generation of alternatively activated macrophages. *Immunity* **23**, 361–374 (2005).
36. E. Sahin, S. Haubenwallner, M. Kuttke, I. Kollmann, A. Halfmann, A. B. Dohnal, L. Chen, P. Cheng, B. Hoesel, E. Einwallner, J. Brunner, J. B. Kral, W. C. Schrottmaier, K. Thell, V. Saferding, S. Blüml, G. Schabbauer, Macrophage PTEN regulates expression and secretion of arginase I modulating innate and adaptive immune responses. *J. Immunol.* **193**, 1717–1727 (2014).
37. J. R. Covvey, E. E. Mancl, Recent evidence for pharmacological treatment of idiopathic pulmonary fibrosis. *Ann. Pharmacother.* **48**, 1611–1619 (2014).
38. M. Gharaee-Kermani, M. R. Gyetko, B. Hu, S. H. Phan, New insights into the pathogenesis and treatment of idiopathic pulmonary fibrosis: A potential role for stem cells in the lung parenchyma and implications for therapy. *Pharm. Res.* **24**, 819–841 (2007).
39. T. C. Carvalho, J. T. McConville, The function and performance of aqueous aerosol devices for inhalation therapy. *J. Pharm. Pharmacol.* **68**, 556–578 (2016).
40. A. Elhissi, Liposomes for pulmonary drug delivery: The role of formulation and inhalation device design. *Curr. Pharm. Design.* **23**, 362–372 (2017).
41. V. Ivanova, O. B. Garbuzenko, K. R. Reuhl, D. C. Reimer, V. P. Pozharov, T. Minko, Inhalation treatment of pulmonary fibrosis by liposomal prostaglandin E2. *Eur. J. Pharm. Biopharm.* **84**, 335–344 (2013).
42. O. B. Garbuzenko, V. Ivanova, V. Kholodovych, D. C. Reimer, K. R. Reuhl, E. Yurkow, D. Adler, T. Minko, Combinatorial treatment of idiopathic pulmonary fibrosis using nanoparticles with prostaglandin E and siRNA(s). *Nanomedicine* **13**, 1983–1992 (2017).
43. K. L. Bajema, A. M. Oster, O. L. McGovern, S. Lindstrom, M. R. Stenger, T. C. Anderson, C. Isenhour, K. R. Clarke, M. E. Evans, V. T. Chu, H. M. Biggs, H. L. Kirking, S. I. Gerber, A. J. Hall, A. M. Fry, S. E. Oliver; 2019-nCoV Persons Under Investigation Team; 2019-CoV Persons Under Investigation Team, Persons evaluated for 2019 Novel Coronavirus – United States, January 2020. *MMWR Morb. Mortal. Wkly. Rep.* **69**, 166–170 (2020).
44. J. Kay, K. S. Upchurch, ACR/EULAR 2010 rheumatoid arthritis classification criteria. *Rheumatology.* **51** (suppl. 6), vi5–vi9 (2012).
45. G. Raghu, H. R. Collard, J. J. Egan, F. J. Martinez, J. Behr, K. K. Brown, T. V. Colby, J.-F. Cordier, K. R. Flaherty, J. A. Lasky, D. A. Lynch, J. H. Ryu, J. J. Swigris, A. U. Wells, J. Ancochea, D. Bouros, C. Carvalho, U. Costabel, M. Ebina, D. M. Hansell, T. Johkoh, D. S. Kim, T. E. King Jr., Y. Kondoh, J. Myers, N. L. Müller, A. G. Nicholson, L. Richeldi, M. Selman, R. F. Dudden, B. S. Griss, S. L. Protzko, H. J. Schünemann; ATS/ERS/JRS/ALAT Committee on Idiopathic Pulmonary Fibrosis, An official ATS/ERS/JRS/ALAT statement: Idiopathic pulmonary fibrosis: Evidence-based guidelines for diagnosis and management. *Am. J. Resp. Crit. Care Med.* **183**, 788–824 (2011).
46. T. Ashcroft, J. M. Simpson, V. Timbrell, Simple method of estimating severity of pulmonary fibrosis on a numerical scale. *J. Clin. Pathol.* **41**, 467–470 (1988).
47. H. Zhang, P. Zhou, Y. Wei, H. Yue, Y. Wang, M. Hu, S. Zhang, T. Cao, C. Yang, M. Li, G. Guo, X. Chen, Y. Chen, M. Lei, H. Liu, J. Zhao, P. Peng, C.-Y. Wang, R. Du, Histopathologic changes and SARS-CoV-2 immunostaining in the lung of a patient with COVID-19. *Ann. Intern. Med.* **172**, 629–632 (2020).
48. Y.-C. Guo, M. Zhang, F.-X. Wang, G.-C. Pei, F. Sun, Y. Zhang, X. He, Y. Wang, J. Song, F.-M. Zhu, N. S. Pandupuspitasari, J. Liu, K. Huang, P. Yang, F. Xiong, S. Zhang, Q. Yu, Y. Yao, C.-Y. Wang, Macrophages regulate unilateral ureteral obstruction-induced renal lymphangiogenesis through C-C motif chemokine receptor 2-dependent phosphatidylinositol 3-kinase-AKT-mechanistic target of rapamycin signaling and hypoxia-inducible factor-1α/vascular endothelial growth factor-C expression. *Am. J. Pathol.* **187**, 1736–1749 (2017).
49. Z. Zhang, L. He, S. Hu, Y. Wang, Q. Lai, P. Yang, Q. Yu, S. Zhang, F. Xiong, S. Simsekyilmaz, Q. Ning, J. Li, D. Zhang, H. Zhang, X. Xiang, Z. Zhou, H. Sun, C.-Y. Wang, AAL exacerbates pro-inflammatory response in macrophages by regulating Mincle/Syk/Card9 signaling along with the Nlrp3 inflammasome assembly. *Am. J. Transl. Res.* **7**, 1812–1825 (2015).
50. L. He, F. Sun, Y. Wang, J. Zhu, J. Fang, S. Zhang, Q. Yu, Q. Gong, B. Ren, X. Xiang, Z. Chen, Q. Ning, J. Hu, P. Yang, C.-Y. Wang, HMGB1 exacerbates bronchiolitis obliterans syndrome via RAGE/NF-κB/HPSE signaling to enhance latent TGF-β release from ECM. *Am. J. Transl. Res.* **8**, 1971–1984 (2016).
51. H. Chen, X. Xu, J. Teng, S. Cheng, H. Bunjhoo, Y. Cao, J. Liu, J. Xie, C. Wang, Y. Xu, W. Xiong, CXCR4 inhibitor attenuates allergen-induced lung inflammation by down-regulating MMP-9 and ERK1/2. *Int. J. Clin. Exp. Pathol.* **8**, 6700–6707 (2015).
52. X. He, Q. Lai, C. Chen, N. Li, F. Sun, W. Huang, S. Zhang, Q. Yu, P. Yang, F. Xiong, Z. Chen, Q. Gong, B. Ren, J. Weng, D. L. Eizirik, Z. Zhou, C.-Y. Wang, Both conditional ablation and overexpression of E2 SUMO-conjugating enzyme (UBC9) in mouse pancreatic beta cells result in impaired beta cell function. *Diabetologia* **61**, 881–895 (2018).
53. P. Yang, Y. Zhang, J. Pang, S. Zhang, Q. Yu, L. He, K.-U. Wagner, Z. Zhou, C.-Y. Wang, Loss of Jak2 impairs endothelial function by attenuating Raf-1/MEK1/Sp-1 signaling along with altered eNOS activities. *Am. J. Pathol.* **183**, 617–625 (2013).
54. X. Fu, F. Sun, F. Wang, J. Zhang, B. Zheng, J. Zhong, T. Yue, X. Zheng, J.-F. Xu, C.-Y. Wang, Aloperine protects mice against DSS-induced colitis by PP2A-mediated PI3K/Akt/mTOR signaling suppression. *Mediators Inflamm.* **2017**, 5706152 (2017).
55. K. A. Whitehead, J. R. Dorkin, A. J. Vegas, P. H. Chang, O. Veiseh, J. Matthews, O. S. Fenton, Y. Zhang, K. T. Olejnik, V. Yesilyurt, D. Chen, S. Barros, B. Klebanov, T. Novobrantseva, R. Langer, D. G. Anderson, Degradable lipid nanoparticles with predictable in vivo siRNA delivery activity. *Nat. Commun.* **5**, 4277 (2014).

Acknowledgments: We are grateful to those patients for donating their BALF and lung tissues for the studies. We are also grateful to W. Mo and S. Liu for breeding the mice for our studies. **Funding:** This study was supported by the National Natural Science Foundation of China (81530024, 91749207, 81920108009, 81770823, 81800068, and 81670729), the Ministry of Science and Technology (2016YFC1305002 and 2017YFC1309603), NHC Drug Discovery Program (2017ZX09304022-07), the Department of Science and Technology of Hubei State (2017ACA096), the Integrated Innovative Team for Major Human Disease Programs of Tongji Medical College, and Huazhong University of Science and Technology. **Author contributions:** Y.W. and L.Z. was responsible for conducting all experiments and data analyses and wrote the manuscript. G.-R.W., H.Y., L.-Z.R., and T.Y. were involved in Western blot, histological analysis, immunostaining, and animal breeding. Q.Z. is responsible for liposome preparation. F.-X.W. and L.-M.C. provided help for flow cytometry. F.S. and J.S. jointly performed some of the experiments. B.M., S.Z., F.X., Q.Y., P.Y., Y.X., and J.Z. were involved in study design and review of the manuscript. H.Z. contributed to discussion and review of the manuscript, study design, and manuscript preparation. W.X. and C.-Y.W. contributed to the study design and manuscript preparation. All authors were involved in drafting the article or revising it critically, and all authors gave their approval for the final manuscript to be published. **Competing interests:** The authors declare that they have no competing interests. **Data and materials availability:** All data needed to evaluate the conclusions in the paper are present in the paper and/or the Supplementary Materials. The data that support the findings of this study are available from the corresponding author upon reasonable request.

Submitted 6 March 2020
Accepted 29 October 2020
Published First Release 4 December 2020
Published 1 January 2021
10.1126/sciadv.abb6075

Citation: Y. Wang, L. Zhang, G.-R. Wu, Q. Zhou, H. Yue, L.-Z. Rao, T. Yuan, B. Mo, F.-X. Wang, L.-M. Chen, F. Sun, J. Song, F. Xiong, S. Zhang, Q. Yu, P. Yang, Y. Xu, J. Zhao, H. Zhang, W. Xiong, C.-Y. Wang, MBD2 serves as a viable target against pulmonary fibrosis by inhibiting macrophage M2 program. *Sci. Adv.* **7**, eabb6075 (2021).